

Charts and atlases for nonlinear data-driven models of dynamics on manifolds

Daniel Floryan and Michael D. Graham*

*Department of Chemical and Biological Engineering,
University of Wisconsin–Madison, Madison, WI 53706, USA*

(Dated: August 16, 2021)

arXiv:2108.05928v1 [cs.LG] 12 Aug 2021

Abstract

We introduce a method for learning minimal-dimensional dynamical models from high-dimensional time series data that lie on a low-dimensional manifold, as arises for many processes. For an arbitrary manifold, there is no smooth global coordinate representation, so following the formalism of differential topology we represent the manifold as an atlas of charts. We first partition the data into overlapping regions. Then undercomplete autoencoders are used to find low-dimensional coordinate representations for each region. We then use the data to learn dynamical models in each region, which together yield a global low-dimensional dynamical model. We apply this method to examples ranging from simple periodic dynamics to complex, nominally high-dimensional non-periodic bursting dynamics of the Kuramoto-Sivashinsky equation. We demonstrate that it: (1) can yield dynamical models of the lowest possible dimension, where previous methods generally cannot; (2) exhibits computational benefits including scalability, parallelizability, and adaptivity; and (3) separates state space into regions of distinct behaviours.

I. INTRODUCTION

Dynamical systems are fundamental to our ability to model processes in engineering and the sciences. Accurate models, in turn, enable deeper understanding of these processes, as well as the ability to predict their future behaviour. In some cases, dynamical models can be derived from first principles; the equations describing how an apple falls under the influence of gravity, for example, can be derived by applying Newton's second law. In other cases, though, no such dynamical models are available. Even when dynamical models can be derived, they may be high-dimensional to the point of being difficult to analyze and prohibitively expensive to make predictions with.

The latter two points have led to great efforts in developing methods that learn low-dimensional dynamical models directly from time series data [1–6]. We focus on the case where rich (high-dimensional) time series data are available, which is increasingly becoming the norm in the era of big data. (Time series that are not sufficiently rich can be augmented via time delay embedding [7].) Such methods typically comprise two modules: one that learns a representation of the state of the system, and another that learns how to evolve

* mdgraham@wisc.edu

the learned state representation forward in time [1–6]. A key enabling assumption is that the data lie on or near a submanifold of the space in which they live, allowing for a state representation of possibly significantly lower dimension than the data while nevertheless containing the same information as the data. Thus, methods of manifold learning feature prominently in this line of work [8–14]. (Notable exceptions to this paradigm are methods inspired by Koopman operator theory, which seek linear dynamical models but require rich state representations in order to be accurate [15–17].)

In this work, we return to the definition of a manifold to learn minimal-dimensional dynamical models from data. A manifold can (and in general must) be described as an atlas of charts: a collection of overlapping patches together with invertible maps between points on the patches and points in Euclidean space [18]. A single patch will not generally suffice—we illustrate with examples below. Several prior works on manifold learning use at least loosely similar ideas, describing a manifold via a collection of local models [19–25]. Brand [23] is the first work we know of that explicitly mentions charts. Like prior works, Brand [23] uses the local models to form a single global parameterization of the manifold, which we will show is limited in the degree of dimension reduction that it can achieve. More recent works follow the atlas of charts representation more closely, avoiding global parameterizations and therefore being able to achieve minimal-dimensional descriptions of manifolds [24, 25]. Nevertheless, the methods in these more recent works would falter in the context of dynamical models: Pitelis *et al.* [24] describe a manifold as a collection of affine subspaces, which would lead to discontinuous dynamics when transitioning between subspaces; similarly, the method of Schonsheck *et al.* [25] would also lead to non-smooth dynamics. Amsallem *et al.* [26] develops a method based on a collection of local affine subspaces that produces continuous dynamics. However, they model the difference between the state at consecutive time steps—not the state itself—as lying in one of several low-dimensional subspaces in their collection. This choice leads to the state living in a higher-dimensional space, diverging from our desire to capture the manifold on which data live.

We propose a method, based on the representation of a manifold as an atlas of charts, that learns smooth minimal-dimensional dynamical models directly from data. We refer to our method as *Charts and Atlases for Nonlinear Data-Driven Dynamics on Manifolds*, and suggest the acronym CANDyMan for short. CANDyMan decomposes a manifold into patches, learns dynamical models on each patch, and sews the local models together to obtain a global

dynamical model without needing a global parameterization. Precise definitions and details of implementation follow. Our examples—ranging from simple low-dimensional periodic dynamics to complex high-dimensional non-periodic bursting dynamics arising in solutions of the Kuramoto-Sivashinsky partial differential equation—will bear out three major benefits of our atlas-of-charts-based framework:

1. The ability to obtain dynamical models of the lowest possible dimension, which previous methods are incapable of.
2. A divide-and-conquer approach that leads to computational benefits including scalability, the ability to adapt models locally, and an embarrassingly parallelizable algorithm.
3. The ability to separate state space into regions of distinct behaviours.

II. A PRIMER ON MANIFOLDS

The word “manifold” evokes an image of a curved surface embedded in a higher-dimensional Euclidean space; this is the relevant scenario for us, in which case our manifolds are, strictly speaking, submanifolds of \mathbb{R}^m . A manifold \mathcal{M} is a set that is locally Euclidean, meaning that every point on the manifold has an open neighbourhood that can be mapped back and forth from and to a Euclidean space \mathbb{R}^n ; the map and its inverse are continuous, and $n \leq m$ is called the dimension of the manifold. Informally, one may think of breaking a manifold into overlapping patches such that each patch can be flattened. This representation is sketched in figure 1, and is formalized by the concept of charts.

A chart is a pair (U, ϕ) , where the coordinate domain U is an open subset of the manifold, and the coordinate map ϕ is a continuous map that maps U to $\phi(U) \subseteq \mathbb{R}^n$ and has a continuous inverse. A point $p \in U$ is mapped to $\phi(p)$, called the local coordinates on U . In general, the coordinate domain of a chart cannot cover the entire manifold, so there will be other charts, and each point on the manifold must belong to the coordinate domain of at least one chart. An atlas is a collection of charts whose coordinate domains cover the manifold, and forms our working representation of a manifold.

To switch between local coordinates, we use transition maps. Given two charts, (U, ϕ) and (V, ψ) , with intersecting coordinate domains, U and V , the transition map from ϕ to ψ

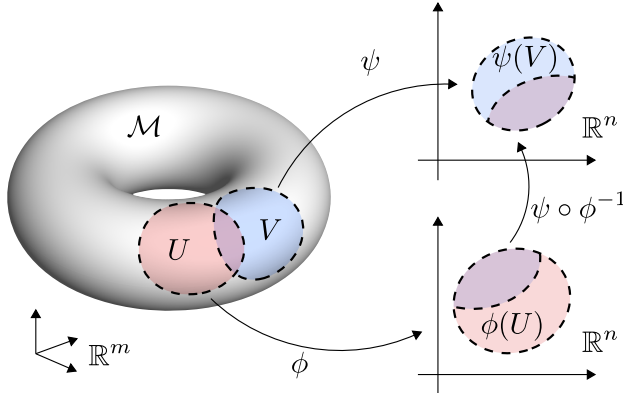


FIG. 1. Two charts, (U, ϕ) and (V, ψ) , of an n -dimensional manifold, \mathcal{M} , embedded in \mathbb{R}^m , and a transition map, $\psi \circ \phi^{-1}$.

is given by $\psi \circ \phi^{-1} : \phi(U \cap V) \rightarrow \psi(U \cap V)$; it is continuous and has continuous inverse. We refer the interested reader to [18] for more details and precise definitions.

A simple circle in the plane elucidates why charts are useful. A circle is a one-dimensional manifold, so we should be able to continuously map back and forth between the circle and \mathbb{R} . But this can only be done locally, not globally, so all popular manifold learning methods will fail at this simple task, producing a discontinuity. Intuitively, these methods try to unwrap a manifold onto a flat surface, but that cannot be done with the circle since it is a closed object. More formally, these methods implicitly use one chart, but at least two charts are needed for a circle.

It is worth pointing out that methods that use one chart, whether implicitly or explicitly, are still able to achieve dimension reduction. The strong Whitney embedding theorem states that any smooth real n -dimensional manifold can be smoothly embedded in \mathbb{R}^{2n} [18, 27]. This means that a one-chart method can theoretically reduce the dimension to $2n$ in the worst case, compared to n for a multi-chart method. Later, we will show an example where our multi-chart method reduces the dimension of data to 3 while nevertheless performing better than a deep autoencoder that reduces the dimension of the data to 6; this result suggests that the practical gap between our multi-chart method and comparable single-chart methods is even greater than the theoretical gap.

III. LEARNING AN ATLAS AND DYNAMICS ON A MANIFOLD

We now describe our method in detail. Suppose we have a dataset generated by a dynamical system. Namely, we have a set of pairs of vectors, $\{(p_i, p'_i)\}_{i=1}^N$, with $p_i, p'_i \in \mathbb{R}^m$, and with p_i mapping to p'_i under the dynamics. This data may be generated by a discrete dynamical system or a continuous dynamical system; in both cases, $p'_i = F(p_i)$ for $i = 1, \dots, N$ for some mapping F (for a continuous dynamical system, we assume that p_i and p'_i are sampled from the continuous dynamical system at times Δt apart for $i = 1, \dots, N$). Usually, such a dataset comes from a single time series $\{p_i\}_{i=1}^{N+1}$, and $p'_i = p_{i+1}$ for $i = 1, \dots, N$.

It is often the case that the dynamical system, and hence the data, live on a submanifold $\mathcal{M} \subset \mathbb{R}^m$ of dimension $n < m$; in some cases, $n \ll m$. We specifically have in mind dissipative systems where at long times, the dynamics approach an invariant manifold. Even for systems described by partial differential equations, which are formally infinite-dimensional, the presence of dissipation can lead to the long-time dynamics residing on a finite-dimensional submanifold [28–30]. Our goal is to learn these manifolds, and the dynamics on them, directly from the data.

The method consists of two steps: first, we learn an atlas of charts; second, we learn the dynamics in the local coordinates of each chart. The key step is to patch the local descriptions together to form a global one. We illustrate the method via the example of a particle moving counterclockwise around the unit circle at constant speed. The data are embedded in \mathbb{R}^2 , but live on the one-dimensional manifold S^1 .

A. Learning an atlas

First, we partition the data into disjoint sets. We use k -means clustering [31–35] to do so. These sets do not yet form the coordinate domains of charts because they do not overlap. To make the sets overlap, we start by building a graph from the data, placing undirected edges between a data point and its K nearest neighbours, for every data point. We then expand each cluster along the graph, giving overlapping coordinate domains and causing some data points to be members of multiple clusters (figure 2A; in this case, each cluster was expanded by two neighbours along the graph). For each cluster, we use that cluster’s

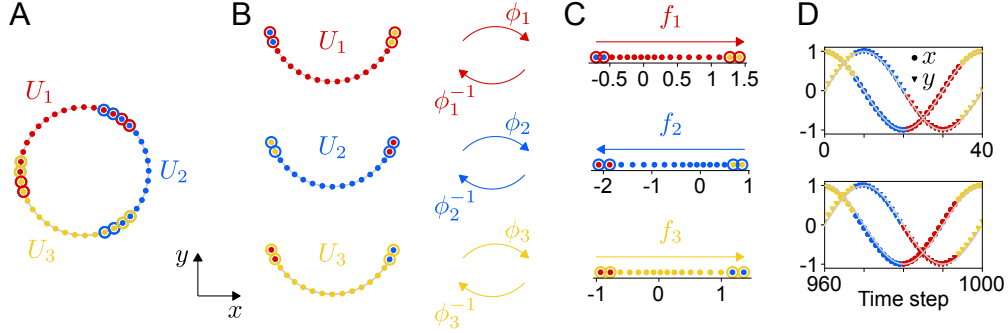


FIG. 2. The method consists of three basic steps: (A) learning coordinate domains (U_1 , U_2 , and U_3 here), (B) learning coordinate maps and their inverses, and (C) learning the dynamics in the local coordinates. In D, we show that the first (top) and 25th (bottom) cycles of motion are well predicted (coloured points are from the learned system, and grey lines are from the true system). Filled markers are interior points, and large open markers are border points.

data to train a deep fully-connected feedforward autoencoder that reduces the dimension of the data to that of the underlying manifold (figure 2B-C). In general, we do not know the dimension of the underlying manifold, so we estimate it by monitoring reconstruction error as a function of dimension. The resulting encoder is the coordinate map of the chart, and the decoder is its approximate inverse. (Other models can be used, for example, principal components analysis can be used to project the data to a lower dimension, and kernel ridge regression used to construct the approximate inverse of that projection.) An approximate transition map between charts is formed by composing the encoder of one chart with the decoder of the other chart.

Note that the ranges of values of the local coordinates differ amongst the three sets of local coordinates in figure 2, and that the densities of the data are not uniform in the local coordinates as they are on the unit circle. The definition of a manifold places no restrictions on the values of the local coordinates; any local coordinates will do as long as the coordinate map is homeomorphic. So, we have not restricted our autoencoders, e.g., by regularizing them in some way. As a result, the sets of local coordinates differ from each other and the distributions of data are distorted by the coordinate maps. In a later example described in section IVE, however, we find that normalizing the local coordinates is helpful when learning dynamics.

B. Learning the dynamics

Now that we have learned an atlas, learning the dynamics is simple. The dynamics on the manifold is given by a map $F_{\mathcal{M}} : \mathcal{M} \rightarrow \mathcal{M}$. In each chart α 's local coordinates, the dynamics are given by $f_{\alpha} = \phi_{\alpha} \circ F_{\mathcal{M}} \circ \phi_{\alpha}^{-1} : \mathbb{R}^n \rightarrow \mathbb{R}^n$. That is, for the chart $(U_{\alpha}, \phi_{\alpha})$ and a point $p \in U_{\alpha}$, the local coordinates of p , $\phi_{\alpha}(p)$, are mapped to $f_{\alpha}(\phi_{\alpha}(p))$ under the dynamics. Learning f_{α} is a simple regression task that gives the low-dimensional dynamics directly. For each chart, we assemble pairs of consecutive data points in that chart and train a deep fully-connected feedforward neural network to map from one point in the pair to the other (figure 2C).

To form a global picture, we need a way to transition between charts under the dynamics. For this purpose, we define the notions of interior and border data points, similar to [24]. We say that a data point is an interior point of a cluster if it was originally assigned to that cluster (filled markers in figure 2A), and we say that a data point is a border point of a cluster if it was assigned to that cluster during the expansion process (open markers in figure 2A). A data point may be a border point of many clusters (or even no clusters), but a data point has a unique interior assignment (as long as the original clustering of data assigned points to unique clusters, as k -means does).

Global dynamics on the manifold works as follows. Starting with an initial condition $p \in \mathcal{M}$, we must find which chart's interior it is in. We find the training data point p_j closest to p . Since p_j belongs to the interior of the coordinate domain of a unique chart α , we use chart α 's coordinate map to map p to that chart's local coordinates, $\phi_{\alpha}(p)$. (Since we use k -means for the clustering step, we may find the cluster centroid that is closest to p instead of the closest training data point.) This initial step is the only one where calculations are performed in the ambient space \mathbb{R}^m . Next, we apply the dynamics that we learned in the local coordinates to map the state forward to $f_{\alpha}(\phi_{\alpha}(p))$. Each time we map the state forward, we find the closest training data point $\phi_{\alpha}(p_k)$ (contained in $\phi_{\alpha}(U_{\alpha})$) in the local coordinates. If p_k is an interior point of the chart, we continue to map the state forward under f_{α} . If p_k is a border point of the chart, instead being uniquely an interior point of chart β , we transition the state to the local coordinates of chart β using the transition map $\phi_{\beta} \circ \phi_{\alpha}^{-1}$, and then proceed similarly, now under the dynamics f_{β} . For example, supposing that our state evolved under chart α 's dynamics for l time steps before transitioning to chart

β , its local coordinates would be $\phi_\beta(\phi_\alpha^{-1}(f_\alpha^l(\phi_\alpha(p))))$. This process is shown in figure 2D for 25 cycles; changes in colour show chart transitions, which appear seamless.

C. Smooth transitions

Let p be a point in the intersection of the coordinate domains of charts α and $\beta \neq \alpha$. Let ϕ_α and ϕ_β denote the coordinate maps that we learn, and let ϕ_α^{inv} and ϕ_β^{inv} denote their approximate inverses that we learn. In order for our model to have smooth dynamics across transitions between charts, we need $\phi_\alpha^{inv}(\phi_\alpha(p))$ and $\phi_\beta^{inv}(\phi_\beta(p))$ to be (nearly) equal for all such p . These are simply the reconstructions of p by the two charts from p 's local coordinates. If they differ significantly, then there will be a discontinuity in the dynamics across transitions. Mathematically, we want to minimize

$$\|\phi_\alpha^{inv}(\phi_\alpha(p)) - \phi_\beta^{inv}(\phi_\beta(p))\| = \|[\phi_\alpha^{inv}(\phi_\alpha(p)) - p] - [\phi_\beta^{inv}(\phi_\beta(p)) - p]\|. \quad (1)$$

The first term in brackets is chart α 's reconstruction error, and the second term is chart β 's reconstruction error. By the triangle inequality,

$$\|[\phi_\alpha^{inv}(\phi_\alpha(p)) - p] - [\phi_\beta^{inv}(\phi_\beta(p)) - p]\| \leq \|\phi_\alpha^{inv}(\phi_\alpha(p)) - p\| + \|\phi_\beta^{inv}(\phi_\beta(p)) - p\|. \quad (2)$$

The difference between the two charts' reconstructions of p is upper-bounded by the sum of each chart's reconstruction error. We can indirectly minimize the difference in the reconstructions by minimizing each chart's reconstruction error. This argument generalizes to multiple points and more than two charts.

By using the triangle inequality, we have decoupled the two charts. We can indirectly minimize the difference in the reconstructions while training our autoencoders separately simply by weighting training data that belong to multiple charts more heavily in each autoencoder's reconstruction loss function. Decoupling the charts allows for trivial parallelization of the training process.

For the results shown in this work, we have not weighted data that belong to multiple charts' coordinate domains more heavily in the autoencoder reconstruction losses. We experimented with doing so, but did not see appreciable effects until the weights were so large that the autoencoders' reconstructions of data belonging to only a single coordinate domain were poor. Nevertheless, this may be an important consideration in future work.

D. Time complexity

The time complexity to map a state forward one time step or to transition from one set of local coordinates to another is the time complexity of a forward pass of the associated neural network(s). This depends on the architectures of the neural networks, but a forward pass of a neural network is typically fast and would be necessary for a traditional one-chart model as well. The major expense comes from searching for a nearest neighbour. Using a k -d tree, the time complexity of a nearest neighbour search is $O(\log_2(N))$ for a constant dimension of the search space [36]. However, the performance degrades rapidly with the dimension of the search space due to the curse of dimensionality, approaching the $O(dN)$ time complexity of brute search in a d -dimensional space once $d \gtrsim 10$ [37]. Fortunately, we only perform a single nearest neighbour search in the high-dimensional ambient space (when assigning the initial condition to a chart), and all subsequent nearest neighbour searches are performed in the local coordinates of the charts.

IV. EXAMPLES

We demonstrate our method on several examples of increasing complexity, from the simple periodic orbit in the plane that we already showed, to complex bursting dynamics of the Kuramoto-Sivashinsky equation. Details about the datasets, neural network architectures, training procedures, and hyperparameters are in the Supplementary Information.

A. Periodic dynamics on a torus

Here we consider a particle moving along the surface of a torus. The particle travels at constant speeds in the poloidal and toroidal directions, three times as fast in the poloidal direction as in the toroidal direction, generating a periodic orbit. The data live on a one-dimensional submanifold of \mathbb{R}^3 , shown in figure 3A.

We place the data into three clusters and follow our procedure to create an atlas of three charts and a local low-dimensional dynamical model for each chart (figure 3A–C). The resulting global dynamical model is excellent. In figure 3D, we show that the learned dynamics (coloured markers) match the true dynamics (grey curves) closely. Note especially the seamless transitions between charts.

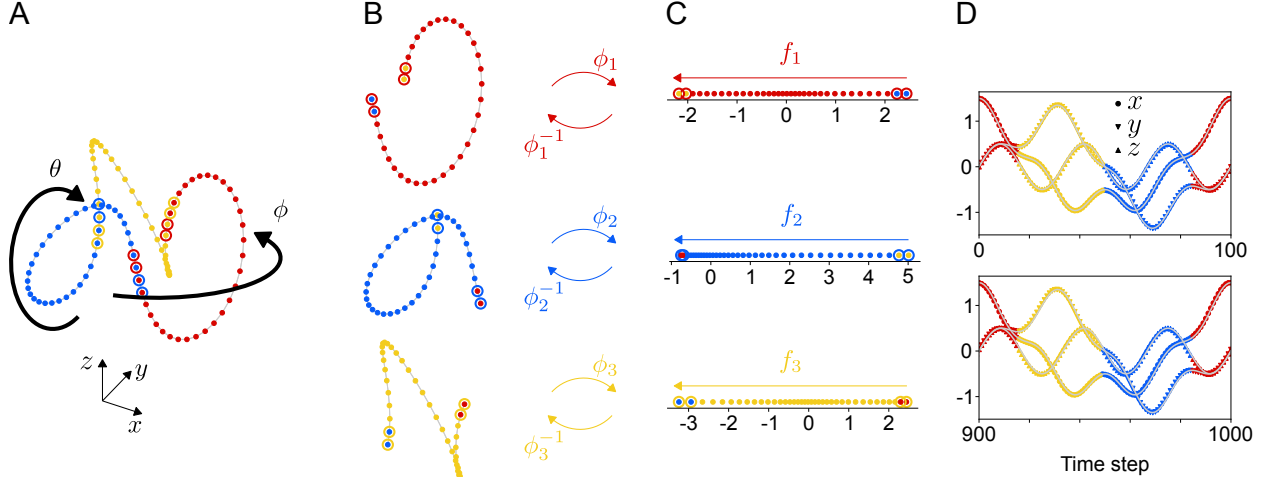


FIG. 3. Analogous to figure 2, but for a periodic orbit on the surface of a torus. In D, we show that the first (top) and tenth (bottom) cycles of motion are well predicted (coloured points are from the learned system, and grey lines are from the true system).

B. Quasiperiodic dynamics on a torus

Now the particle travels in the poloidal direction $\sqrt{3}$ times as fast as in the toroidal direction. Since the speeds are incommensurate, the particle's orbit is quasiperiodic, densely filling the surface of the torus in the limit of infinite time. The data live on a two-dimensional submanifold of \mathbb{R}^3 , shown in figure 4A.

We place the data into six clusters and follow our procedure to create an atlas of six charts and a local low-dimensional dynamical model for each chart (figure 4A–C). The choice of six charts is arbitrary; as few as three (specially chosen) charts will work in this case. Note that some of the data points are assigned to up to four charts.

In figure 4D, we show the trajectory that results from evolving an initial condition forward under our learned dynamical model. The learned dynamics are generally correct, but the phase speeds are a little bit off (roughly 0.5% too slow in the poloidal direction and 0.5% too fast in the toroidal direction). The transitions between charts are apparently quite smooth, even when a chart is visited for only one time step (around time step 55). When we analyze first and higher order differences between consecutive points produced by our learned dynamical model, hiccups become apparent when transitioning between charts. This is to be expected since the decoders only approximate the encoders' inverses, as discussed

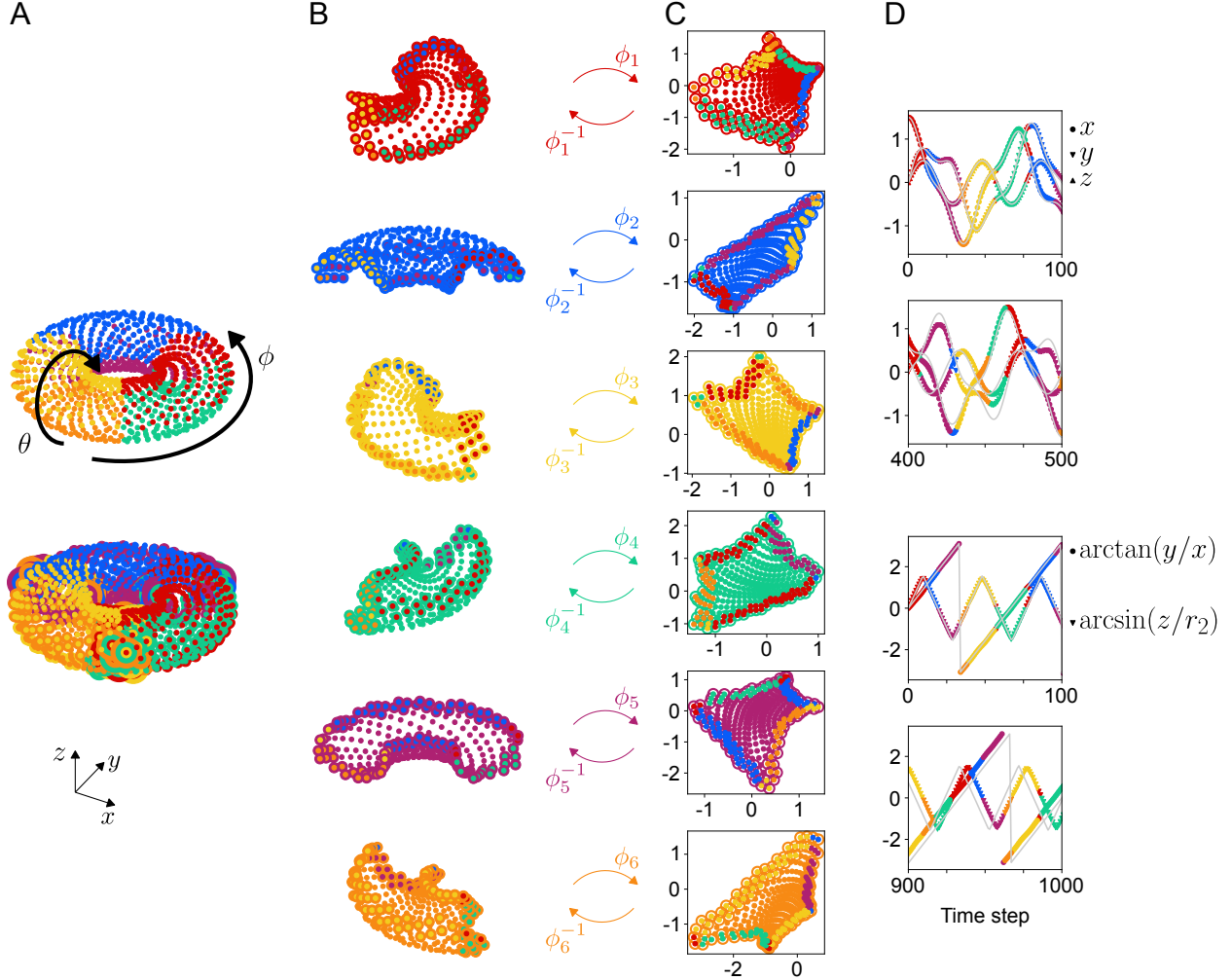


FIG. 4. Analogous to figure 2, but for a quasiperiodic orbit on the surface of a torus. In A, we show the data before and after coordinate domains are made to overlap; data belong to up to four coordinate domains. In D, we show that the dynamics are well predicted (coloured points are from the learned system, and grey lines are from the true system). The top two plots show the predicted Cartesian coordinates on the surface of the torus, and the bottom two plots show the predicted poloidal and toroidal coordinates.

in section III C.

For the learned model whose results are shown in figure 4, we are confident that it indeed has quasiperiodic dynamics (we used the model to produce a trajectory that is 50,000 time steps long, finding no repeating pattern). However, the majority of the time we learn models that have periodic dynamics, with the period being on the order of the number of training

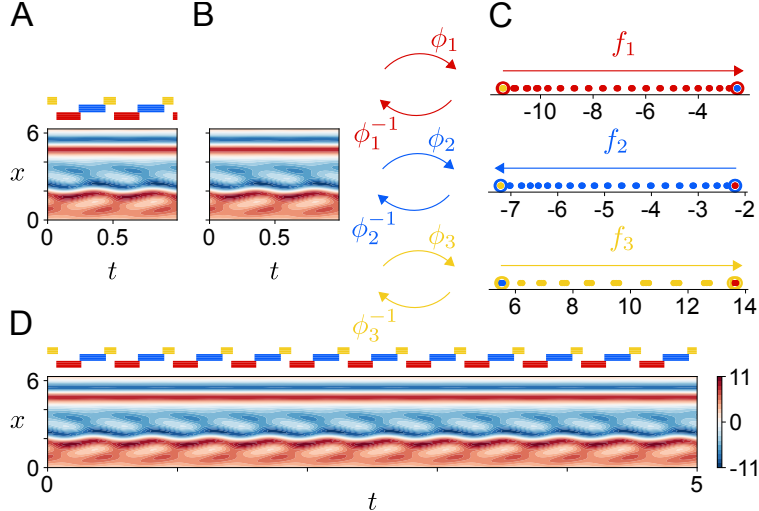


FIG. 5. Analogous to figure 2, but for a beating standing wave from the K-S system. The coloured bars in A show which chart the data belong to, and B shows the result of putting the data through the autoencoders. In D, we show that the periodic dynamics are well predicted.

data but varying fairly significantly (ten learned models with periodic dynamics had periods between 418 and 1892 time steps). We attribute this to the existence of Arnold tongues, leading to a phase locking (or mode locking) phenomenon that often causes our learned model to have periodic dynamics. In short, if the dynamics of a nominally quasiperiodic system are perturbed, then the dynamics will be periodic in a finite region of parameter values; see [38] for more details.

C. Beating dynamics

Our next example comes from the Kuramoto-Sivashinsky (K-S) partial differential equation,

$$u_t + uu_x + u_{xx} + \nu u_{xxxx} = 0, \quad (3)$$

for $0 \leq x \leq 2\pi$, with periodic boundary conditions. We set $\nu = \frac{16}{337}$ [39] and compute a numerical solution using a pseudo-spectral method with 64 Fourier modes. After transients have died out, we obtain a beating standing wave. The data live on a one-dimensional submanifold of \mathbb{R}^{64} , shown in figure 5A.

We place the data into three clusters and follow our procedure to create an atlas of three

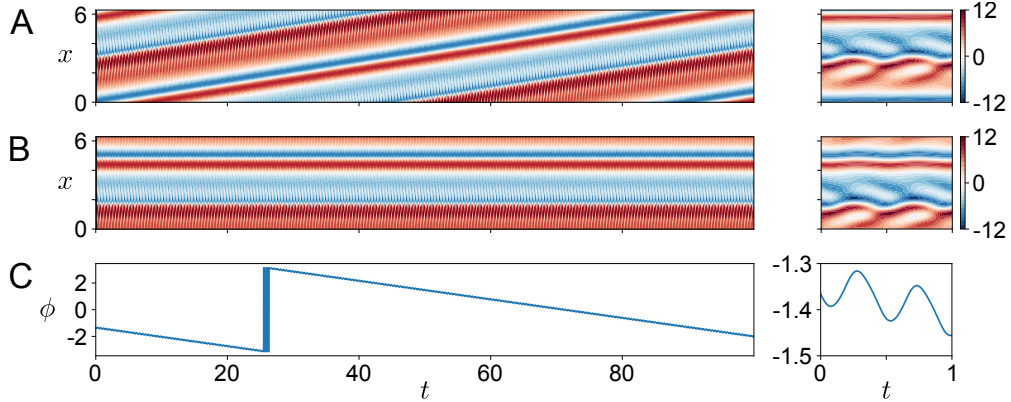


FIG. 6. The beating travelling wave data from the K-S system (A) are separated into shape (B) and phase (C) data. Plots on the right show close-up views of the first time unit of the dynamics.

charts and a local low-dimensional dynamical model for each chart (figure 5A–C). Figure 5B shows the reconstruction of the data from their local coordinates, demonstrating excellent reconstruction.

In figure 5D, we show a trajectory that results from evolving an initial condition forward in time under our learned dynamical model. The transitions between charts are seamless and the trajectory is indistinguishable from the data. This example demonstrates that our method works in higher dimensions, producing a minimal one-dimensional dynamical model for nominally 64-dimensional data.

D. Beating travelling dynamics

Our next example also comes from the K-S equation, this time with $\nu = \frac{4}{87}$ [39]. After transients have died out, we obtain a beating travelling wave. The travelling period and beating period are incommensurable, making the orbit quasiperiodic. Note the separation in timescales: the two periods differ by a factor of nearly 200. This quasiperiodic orbit lives on a two-dimensional submanifold (a 2-torus) of \mathbb{R}^{64} , shown in figure 6A.

We separate the data into shape (figure 6B) and phase (figure 6C) variables (the shape variable’s first Fourier mode’s phase is zero) [6, 40]. Because of the translational equivariance of (3), the dynamics only depend on the shape variable, which lives on a one-dimensional submanifold of \mathbb{R}^{64} .

Our training data are shown in figure 7A. The data span a bit more than two beating

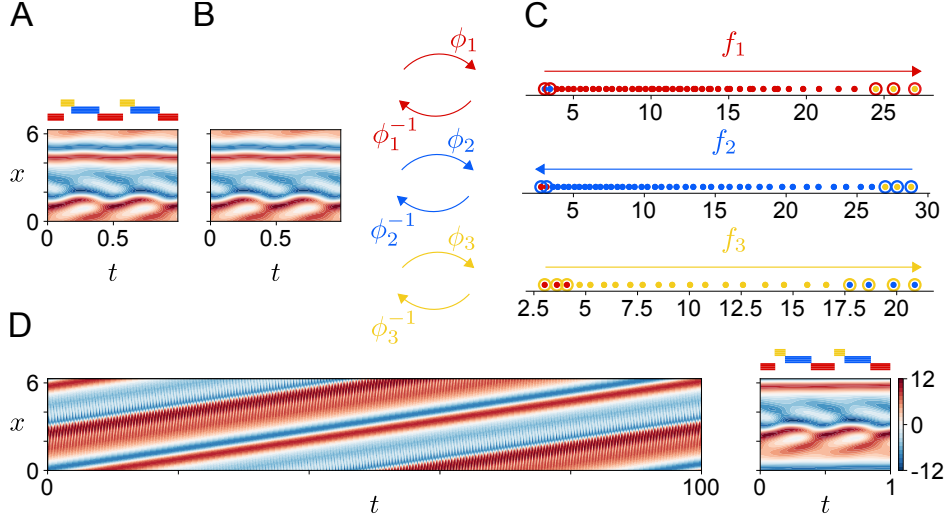


FIG. 7. Analogous to figure 5, but for a beating travelling wave. In D, we show the predicted dynamics starting from the same initial condition as in figure 6A.

periods, just over 1% of the travelling period. We place the data into three clusters and follow our procedure to create an atlas of three charts and a local low-dimensional dynamical model for each chart (figure 7A–C). Additionally, for each chart we train a neural network that takes the shape variable (in local coordinates) as input and predicts the change in phase over one time step, giving the phase dynamics [6].

In figure 7D, we show a trajectory that results from evolving an initial condition forward in time under our learned dynamical model. Comparing figure 7D to figure 6A, our learned model again produces good results with seamless transitions between charts. The beating period of our model is 0.456 ± 0.001 time units, identical to the data, and the travelling period of our model is 94.88 ± 0.10 time units, compared to 90.46 ± 0.10 time units for the data. The discrepancy improves with increased training time of the neural networks.

It is worth re-iterating that the two periods of the quasiperiodic data differ by a factor of almost 200. Despite the large separation in timescales, our method produced a good dynamical model. Moreover, we were able to take advantage of a symmetry present in the system to reduce the data to a one-dimensional representation while still obtaining quasiperiodic dynamics, and learn from data that spans a small fraction of one of the timescales while nevertheless capturing that timescale in the final dynamical model.

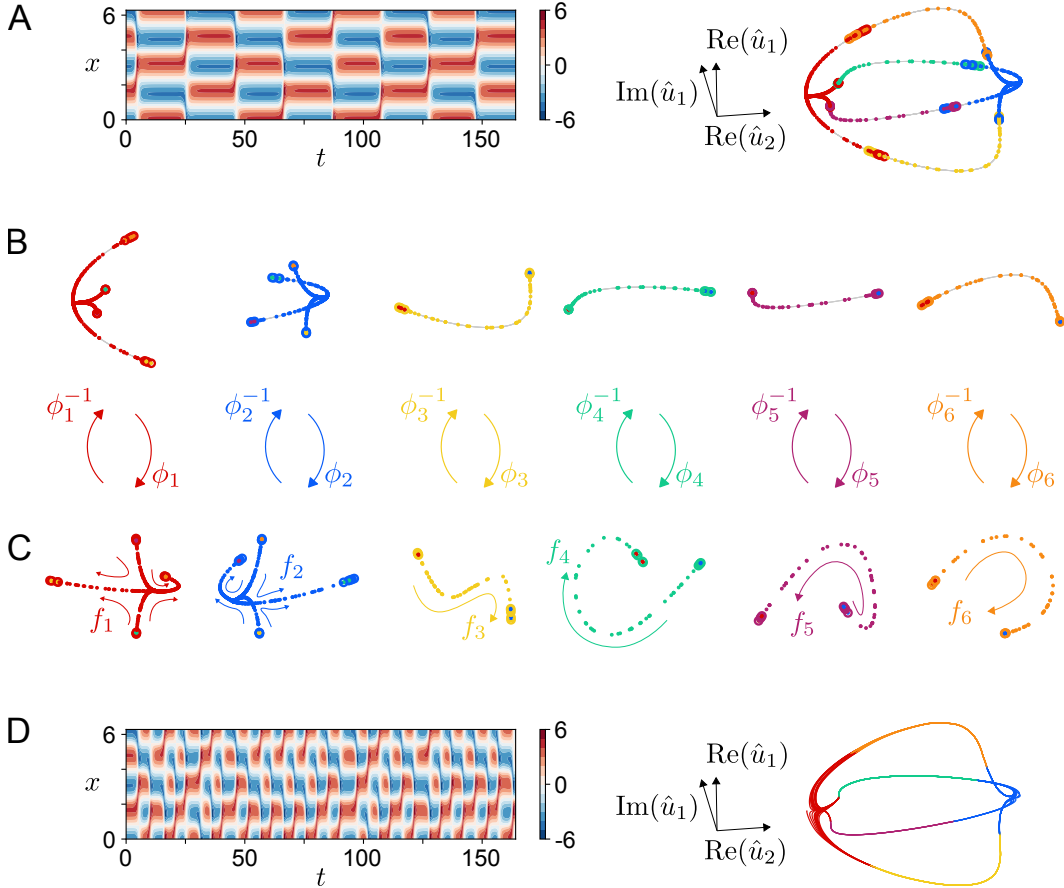


FIG. 8. Analogous to figure 2, but for bursting data from the K-S system. In A and D, we show space-time plots and projections onto the real part of the second spatial Fourier mode and real and imaginary parts of the first spatial Fourier mode. Note that B shows a projection of the data, whereas C shows the data in the full learned three-dimensional spaces. In A-C, we subsampled the data for visual clarity.

E. Bursting dynamics

Our final example comes from the K-S equation with $\nu = \frac{16}{71}$ [41]. After transients have died out, we obtain complicated bursting dynamics, shown in figure 8A. The field bursts between pseudo-steady cellular states of opposite sign. The state space projection clarifies that the state seems to switch between two saddle points that are connected by four heteroclinic orbits [42]. The trajectory is non-periodic, as the state travels along each heteroclinic orbit pseudo-randomly with equal probability.

Our data cover each heteroclinic orbit four times, with the first half shown in figure 8A.

The data live on a submanifold of unknown dimension. We will use our method to find the dimension of the submanifold, and compare the results to a one-chart model.

We place the data into six clusters and follow our procedure to create an atlas of six charts and a local low-dimensional dynamical model for each chart (figure 8A–C). We chose to use six charts based on the state space structure in figure 8A. The clusters respectively constitute the two saddle points and the four heteroclinic orbits; this clustering of the data was done automatically by k -means.

We successfully built a model with three-dimensional local coordinates. In order to recreate qualitatively correct dynamics, we had to use the method described in [6] for the autoencoders, and normalize the local coordinates before learning the dynamics. The normalization we used is similar to whitening, with full details in the Supplementary Information. Additionally, we also had to use a different dataset with off-attractor data to train the neural networks for dynamics; details are in the Supplementary Information. The reason for using off-attractor data to learn the dynamics is that the attractor is very thin (see figure 8C), making it difficult to learn accurate dynamics in the three-dimensional local coordinates. When only using the original dataset to learn the dynamics, we found that the learned dynamics often included a stable fixed point that was off the attractor (in a region where there was no data to learn from). The new dynamics dataset was partitioned and transformed to local coordinates based on the previously trained charts before training the neural networks for the dynamics.

Even with the above modifications, many of our learned models display periodic dynamics. We have found models that have one stable limit cycle (essentially consisting of two of the heteroclinic orbits), two stable limit cycles (each consisting of an independent pair of the heteroclinic orbits), and one longer stable limit cycle (consisting of all four heteroclinic orbits), in addition to models with non-periodic dynamics. We attribute this to the presence, in the space of weights for the neural networks for the dynamics, of a gluing bifurcation [43–45]. In short, perturbations to the dynamics can “glue” the heteroclinic orbits together, forming periodic orbits of various degrees of complexity. It may be possible to avoid the gluing bifurcation by enforcing some of the symmetries present in the K-S system [42], but we do not pursue this avenue here. Figure 8 and the discussion below describe results from a model that does display qualitatively correct non-periodic dynamics.

In figure 8D, we show a trajectory that results from evolving an initial condition forward

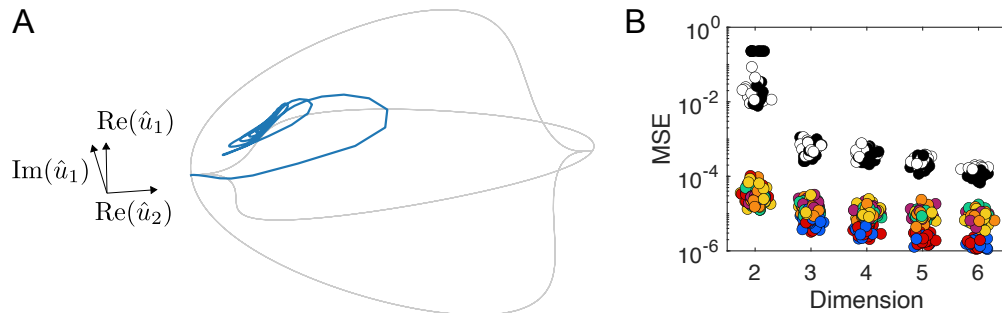


FIG. 9. (A) Dynamics produced by a one-chart model with six-dimensional local coordinates (solid blue line). The true attractor is shown with a thin grey line. (B) MSEs of autoencoders of various bottleneck dimensions when trained on the bursting K-S data, using six charts (coloured markers, colours as in figure 8) and one chart (black and white markers). Autoencoders corresponding to black markers have the same architecture as those used in the six-chart case. Autoencoders corresponding to white markers have approximately the same number of trainable parameters as all six autoencoders in total from the six-chart case. For all cases, 20 trials were performed.

under our learned three-dimensional dynamical model. We are able to obtain qualitatively correct non-periodic bursting dynamics. The quasi-steady cellular states quantitatively match those in the original data. The only quantitative discrepancy is in how long the state stays in a quasi-steady cellular state. This difference can be understood from the fact that these quasi-steady states are approaches to saddle points. The time that a trajectory spends near a saddle point scales as $-\ln y$ near the saddle point, where y is the distance from the stable manifold of the trajectory. The logarithmic divergence explains the sensitivity of the quiescent periods to model error.

For comparison, in figure 9A we show a typical trajectory that results from a one-chart model with six-dimensional local coordinates. The state settles onto a fixed point in the model, not reflective of the true dynamics. Although higher-dimensional one-chart models are in principle capable of capturing the attractor (by the strong Whitney embedding theorem), as a practical matter, we find that they are unable to capture the qualitative dynamics of this complex system.

Besides being able to capture dynamics that one-chart models are unable to, our multi-chart method also captures the submanifold better. In figure 9B, we show the mean squared errors (MSEs) of several autoencoders (using the method in [6]) as a function of the di-

mension of the local coordinates. The six-chart atlases (coloured markers) produce MSEs that are consistently over an order of magnitude lower than those of the one-chart atlases (black and white markers). The key comparison to make is between the six-chart atlas with three-dimensional local coordinates, and the one-chart atlas with six-dimensional local coordinates. Since the submanifold is three-dimensional, the strong Whitney embedding theorem states that it can be smoothly embedded in \mathbb{R}^6 , i.e., it can be captured by a one-chart atlas with six-dimensional local coordinates. Nevertheless, the MSE of the six-chart atlas is an order of magnitude lower than that of the one-chart atlas with twice the dimension and same number of trainable parameters. It is clear that our multi-chart method provides practical benefits even beyond what is theoretically predicted.

V. CONCLUSIONS

We introduced a method that is able to learn smooth minimal-dimensional dynamical models directly from high-dimensional time series data. Our approach first finds and parameterizes the low-dimensional manifold on which the data live, then learns the dynamics on that manifold.

Taking inspiration from the general mathematical representation of a manifold, we characterize learning a manifold as learning an atlas of charts: a collection of overlapping patches on the manifold together with invertible maps between points on the patches and points in Euclidean space. We implement an atlas of charts by clustering the data in state space to form patches, assigning a deep autoencoder to each patch for the dimension reduction step, and using deep neural networks to learn the dynamics in each patch. Finally, we sew the local models together to obtain a global dynamical model. We call our method CANDyMan, short for charts and atlases for nonlinear data-driven dynamics on manifolds.

We applied CANDyMan to six examples of varying complexity, demonstrating that it: (1) has the ability to obtain dynamical models of the lowest possible dimension, which previous methods are incapable of; (2) uses a divide-and-conquer approach that leads to computational benefits including scalability, the ability to adapt models locally, and an embarrassingly parallelizable algorithm; and (3) has the ability to separate state space into regions of distinct behaviours. When applied to complicated bursting data generated by the Kuramoto-Sivashinsky partial differential equation, CANDyMan produced a three-

dimensional dynamical model with qualitatively and semi-quantitatively correct dynamics, while even a six-dimensional single-chart method did not succeed, producing qualitatively incorrect behaviour. Likewise, the three-dimensional CANDyMan model had an order of magnitude lower error when reconstructing data from their low-dimensional representations than an autoencoder with the same number of trainable parameters and a bottleneck dimension of six. This shows that CANDyMan has practical benefits beyond what is theoretically predicted by the strong Whitney embedding theorem.

A question that naturally arises is how many charts must be used. This question is intimately tied to the dimension that we are able to reduce the data to. We may always use a single chart, but doing so limits the dimension reduction that can be achieved. How many charts do we need in order to obtain a minimal-dimensional representation of the data, and how do we know what the minimal dimension is? For now, we suggest an empirical approach where one would sample in the space of number of charts and number of dimensions. It may be easier to first find the appropriate dimension by only considering a low number of charts that cover small incomplete patches of the data, and tuning the dimension of these charts; since the dimension of a manifold is a global property, it can be established locally in this way. Once the appropriate dimension is found, the number of charts can be tuned empirically.

We wish to emphasize that the application of deep learning and k -means should not be read as the contributions of this work. Rather, the true contribution of our work is the broader use and implementation of an atlas of charts in the context of dynamics. It may well be that other methods of partitioning data and learning charts (and associated transition maps) are better and more efficient; this deserves consideration in future work, and would fall under the CANDyMan framework. In particular, although the theory of manifolds is agnostic to what form the coordinate maps take (as long as they are homeomorphisms), from a practical standpoint, we believe that imposing structure on the coordinate maps will make learning the correct dynamics easier, as we saw in our last example. What this structure should be deserves more attention than our ad hoc attempt.

Finally, because our method decomposes state space into patches, we believe that it is particularly suited to applications that display very different behaviours in different parts of state space, such as the bursting and intermittency characteristic of turbulent fluid flows.

ACKNOWLEDGEMENTS

This work was supported by AFOSR grant FA9550-18-0174 and ONR grant N00014-18-1-2865 (Vannevar Bush Faculty Fellowship).

AUTHOR CONTRIBUTIONS

D.F. and M.D.G. designed research, performed research, analyzed data, and wrote the paper.

COMPETING INTERESTS

The authors declare no competing interests.

-
- [1] N. Watters, D. Zoran, T. Weber, P. Battaglia, R. Pascanu, and A. Tacchetti, Visual interaction networks: Learning a physics simulator from video, in *Advances in Neural Information Processing Systems*, Vol. 30, edited by I. Guyon, U. V. Luxburg, S. Bengio, H. Wallach, R. Fergus, S. Vishwanathan, and R. Garnett (Curran Associates, Inc., 2017).
 - [2] F. J. Gonzalez and M. Balajewicz, Deep convolutional recurrent autoencoders for learning low-dimensional feature dynamics of fluid systems, arXiv preprint arXiv:1808.01346 (2018).
 - [3] P. R. Vlachas, W. Byeon, Z. Y. Wan, T. P. Sapsis, and P. Koumoutsakos, Data-driven forecasting of high-dimensional chaotic systems with long short-term memory networks, *Proceedings of the Royal Society A: Mathematical, Physical and Engineering Sciences* **474**, 20170844 (2018).
 - [4] K. Champion, B. Lusch, J. N. Kutz, and S. L. Brunton, Data-driven discovery of coordinates and governing equations, *Proceedings of the National Academy of Sciences* **116**, 22445 (2019).
 - [5] K. T. Carlberg, A. Jameson, M. J. Kochenderfer, J. Morton, L. Peng, and F. D. Witherden, Recovering missing CFD data for high-order discretizations using deep neural networks and dynamics learning, *Journal of Computational Physics* **395**, 105 (2019).
 - [6] A. J. Linot and M. D. Graham, Deep learning to discover and predict dynamics on an inertial manifold, *Physical Review E* **101**, 062209 (2020).

- [7] F. Takens, Detecting strange attractors in turbulence, in *Dynamical Systems and Turbulence, Warwick 1980*, edited by D. Rand and L.-S. Young (Springer Berlin Heidelberg, Berlin, Heidelberg, 1981) pp. 366–381.
- [8] B. Schölkopf, A. Smola, and K.-R. Müller, Nonlinear component analysis as a kernel eigenvalue problem, *Neural Computation* **10**, 1299 (1998).
- [9] J. B. Tenenbaum, V. De Silva, and J. C. Langford, A global geometric framework for nonlinear dimensionality reduction, *Science* **290**, 2319 (2000).
- [10] S. T. Roweis and L. K. Saul, Nonlinear dimensionality reduction by locally linear embedding, *Science* **290**, 2323 (2000).
- [11] M. Belkin and P. Niyogi, Laplacian eigenmaps for dimensionality reduction and data representation, *Neural Computation* **15**, 1373 (2003).
- [12] D. L. Donoho and C. Grimes, Hessian eigenmaps: Locally linear embedding techniques for high-dimensional data, *Proceedings of the National Academy of Sciences* **100**, 5591 (2003).
- [13] L. van der Maaten and G. Hinton, Visualizing data using t-SNE, *Journal of Machine Learning Research* **9** (2008).
- [14] I. Goodfellow, Y. Bengio, and A. Courville, *Deep Learning* (MIT Press, 2016).
- [15] N. Takeishi, Y. Kawahara, and T. Yairi, Learning Koopman invariant subspaces for dynamic mode decomposition, in *Advances in Neural Information Processing Systems*, Vol. 30, edited by I. Guyon, U. V. Luxburg, S. Bengio, H. Wallach, R. Fergus, S. Vishwanathan, and R. Garnett (2017).
- [16] B. Lusch, J. N. Kutz, and S. L. Brunton, Deep learning for universal linear embeddings of nonlinear dynamics, *Nature Communications* **9**, 1 (2018).
- [17] S. E. Otto and C. W. Rowley, Linearly recurrent autoencoder networks for learning dynamics, *SIAM Journal on Applied Dynamical Systems* **18**, 558 (2019).
- [18] J. M. Lee, *Introduction to Smooth Manifolds* (Springer, 2013).
- [19] C. Bregler and S. Omohundro, Surface learning with applications to lipreading, in *Advances in Neural Information Processing Systems*, Vol. 6, edited by J. Cowan, G. Tesauro, and J. Al-spector (Morgan-Kaufmann, 1994).
- [20] G. E. Hinton, M. Revow, and P. Dayan, Recognizing handwritten digits using mixtures of linear models, in *Advances in Neural Information Processing Systems*, Vol. 7, edited by G. Tesauro, D. Touretzky, and T. Leen (MIT Press, 1995).

- [21] N. Kambhatla and T. K. Leen, Dimension reduction by local principal component analysis, *Neural Computation* **9**, 1493 (1997).
- [22] S. Roweis, L. Saul, and G. E. Hinton, Global coordination of local linear models, in *Advances in Neural Information Processing Systems*, Vol. 14, edited by T. Dietterich, S. Becker, and Z. Ghahramani (MIT Press, 2002).
- [23] M. Brand, Charting a manifold, in *Advances in Neural Information Processing Systems*, Vol. 15, edited by S. Becker, S. Thrun, and K. Obermayer (MIT Press, 2003) pp. 985–992.
- [24] N. Pitelis, C. Russell, and L. Agapito, Learning a manifold as an atlas, in *Proceedings of the IEEE Conference on Computer Vision and Pattern Recognition* (2013) pp. 1642–1649.
- [25] S. Schonsheck, J. Chen, and R. Lai, Chart auto-encoders for manifold structured data, arXiv preprint arXiv:1912.10094 (2019).
- [26] D. Amsallem, M. J. Zahr, and C. Farhat, Nonlinear model order reduction based on local reduced-order bases, *International Journal for Numerical Methods in Engineering* **92**, 891 (2012).
- [27] H. Whitney, The self-intersections of a smooth n -manifold in $2n$ -space, *Annals of Mathematics* , 220 (1944).
- [28] E. Hopf, A mathematical example displaying features of turbulence, *Communications on Pure and Applied Mathematics* **1**, 303 (1948).
- [29] R. Temam and X. M. Wang, Estimates on the lowest dimension of inertial manifolds for the Kuramoto-Sivashinsky equation in the general case, *Differential and Integral Equations* **7**, 1095 (1994).
- [30] C. R. Doering and J. D. Gibbon, *Applied Analysis of the Navier-Stokes Equations*, Cambridge Texts in Applied Mathematics No. 12 (1995).
- [31] J. MacQueen, Some methods for classification and analysis of multivariate observations, in *Proceedings of the Fifth Berkeley Symposium on Mathematical Statistics and Probability*, Vol. 5.1, edited by L. M. Le Cam and J. Neyman (Statistical Laboratory of the University of California, Berkeley, 1967) pp. 281–297.
- [32] H. Steinhaus, Sur la division des corps matériels en parties, *Bull. Acad. Polon. Sci* **4**, 801 (1957).
- [33] S. Lloyd, Least squares quantization in PCM, *IEEE Transactions on Information Theory* **28**, 129 (1982).

- [34] E. W. Forgy, Cluster analysis of multivariate data: efficiency versus interpretability of classifications, *Biometrics* **21**, 768 (1965).
- [35] F. Pedregosa, G. Varoquaux, A. Gramfort, V. Michel, B. Thirion, O. Grisel, M. Blondel, P. Prettenhofer, R. Weiss, V. Dubourg, J. Vanderplas, A. Passos, D. Cournapeau, M. Brucher, M. Perrot, and E. Duchesnay, Scikit-learn: Machine learning in Python, *Journal of Machine Learning Research* **12**, 2825 (2011).
- [36] J. H. Friedman, J. L. Bentley, and R. A. Finkel, An algorithm for finding best matches in logarithmic expected time, *ACM Transactions on Mathematical Software (TOMS)* **3**, 209 (1977).
- [37] R. Weber, H.-J. Schek, and S. Blott, A quantitative analysis and performance study for similarity-search methods in high-dimensional spaces, in *VLDB'98, Proceedings of 24th International Conference on Very Large Data Bases, August 24-27, 1998, New York City, New York, USA*, edited by A. Gupta, O. Shmueli, and J. Widom (Morgan Kaufmann, 1998) pp. 194–205.
- [38] S. Wiggins, *Introduction to Applied Nonlinear Dynamical Systems and Chaos*, 2nd ed. (Springer-Verlag New York, 2003).
- [39] C. W. Rowley and J. E. Marsden, Reconstruction equations and the Karhunen–Loève expansion for systems with symmetry, *Physica D: Nonlinear Phenomena* **142**, 1 (2000).
- [40] N. B. Budanur, P. Cvitanović, R. L. Davidchack, and E. Siminos, Reduction of $SO(2)$ symmetry for spatially extended dynamical systems, *Physical Review Letters* **114**, 084102 (2015).
- [41] M. Kirby and D. Armbruster, Reconstructing phase space from PDE simulations, *Zeitschrift für angewandte Mathematik und Physik ZAMP* **43**, 999 (1992).
- [42] I. G. Kevrekidis, B. Nicolaenko, and J. C. Scovel, Back in the saddle again: a computer assisted study of the Kuramoto–Sivashinsky equation, *SIAM Journal on Applied Mathematics* **50**, 760 (1990).
- [43] J.-M. Gambaudo, P. Glendinning, and C. Tresser, Collage de cycles et suites de Farey, *Comptes rendus des séances de l'Académie des sciences, Série 1, Mathématique* **299**, 711 (1984).
- [44] P. Glendinning, Global bifurcations in flows, in *New Directions in Dynamical Systems*, London Mathematical Society Lecture Note Series, Vol. 127, edited by T. Bedford and J. Swift (Cambridge University Press, Cambridge, 1988) pp. 120–149.

- [45] M. D. Graham, U. Middy, and D. Luss, Pulses and global bifurcations in a nonlocal reaction-diffusion system, *Physical Review E* **48**, 2917 (1993).
- [46] F. Chollet *et al.*, Keras, <https://keras.io> (2015).
- [47] D. P. Kingma and J. Ba, Adam: A method for stochastic optimization, arXiv preprint arXiv:1412.6980 (2014).
- [48] X. Glorot and Y. Bengio, Understanding the difficulty of training deep feedforward neural networks, in *Proceedings of the Thirteenth International Conference on Artificial Intelligence and Statistics* (JMLR Workshop and Conference Proceedings, 2010) pp. 249–256.

Supplementary Information for Floryan and Graham, Charts and atlases for nonlinear data-driven models of dynamics on manifolds

The Supplementary Information contains details about the training datasets, neural network architectures, training procedures, and hyperparameters used for each of the examples in the main text. Neural networks were built and trained using Keras [46]. Unless otherwise indicated, all neural network layers are fully-connected, the mean squared error is used as the loss function, the default Adam optimizer is used for training [47], the default Glorot uniform initializer is used for weight initialization [48], and the batch size is the full number of training data points in the corresponding chart.

We did not attempt to optimize architectures nor hyperparameters, simply using ones that produced accurate results. To choose the dimension of the local coordinates, we either knew what the true dimension of the submanifold was (in which case we used that dimension), or we based our decision on reconstruction errors (i.e., figure 9B in the main text suggests that the dimension of the bursting data is 3 since the reconstruction error reaches a plateau there [6]; note that the dimension cannot be 2 since such a low dimension is not capable of producing the dynamics we observe). To choose the number of charts, we often knew the minimum number needed, and chose nearly that many. For the bursting example, we chose to use 6 charts based on an exploratory data analysis, where we saw that the state space structure of the data consists of two saddles connected by four heteroclinic orbits.

S1. PERIODIC DYNAMICS ON A CIRCLE

The training data are the Cartesian (x, y) coordinates of a particle as it moves counter-clockwise around the unit circle at a constant speed. There are 40 data points in total, uniformly spaced $\pi/20$ radians apart on the unit circle.

We use three charts (three clusters in k -means). The graph is built by connecting points to their two nearest neighbours. Clusters are expanded twice along the graph.

The neural network parameters are listed in table I. The autoencoders are trained with a learning rate of 0.01, and the neural networks for dynamics are trained with a learning rate of 0.005.

	Shape	Activations	Epochs
Encoders	2 : 32 : 32 : 16 : 4 : 1	elu : elu : elu : elu : linear	1000
Decoders	1 : 4 : 16 : 32 : 32 : 2	elu : elu : elu : elu : linear	1000
Dynamics	1 : 32 : 32 : 16 : 4 : 1	elu : elu : elu : elu : linear	500

TABLE I. Neural network parameters for periodic dynamics on a circle. “Shape” indicates the dimension of each layer, “activation” indicates the activation functions between layers, and “epochs” indicates the number of epochs used for training.

S2. PERIODIC DYNAMICS ON A TORUS

The training data are the Cartesian (x, y, z) coordinates of a particle as it moves around the surface of a torus. The surface of the torus is given by

$$x = (1 + 0.5 \cos \theta) \cos \phi, \quad y = (1 + 0.5 \sin \theta) \sin \phi, \quad z = 0.5 \sin \theta, \quad (\text{S1})$$

where θ is the poloidal coordinate and ϕ is the toroidal coordinate. The particle moves at a constant rate in the poloidal and toroidal directions, three times as fast in the poloidal direction, generating a periodic orbit. There are 100 data points in total, uniformly spaced $\pi/50$ radians apart in the toroidal direction, covering one full period of the motion.

We use three charts (three clusters in k -means). The graph is built by connecting points to their two nearest neighbours. Clusters are expanded twice along the graph.

The neural network parameters are listed in table II. The autoencoders are trained with an exponential decay learning rate schedule (initial learning rate 0.01, decay rate 0.9 every 200 steps using a staircase function), and the neural networks for dynamics are also trained with an exponential decay learning rate schedule (initial learning rate 0.01, decay rate 0.9 every 200 steps using a staircase function).

S3. QUASIPERIODIC DYNAMICS ON A TORUS

The training data are the Cartesian (x, y, z) coordinates of a particle as it moves around the surface of a torus. The surface of the torus is given by (S1). The particle moves at a constant rate in the poloidal and toroidal directions, $\sqrt{3}$ times as fast in the poloidal direction, generating a quasiperiodic orbit. There are 1000 data points in total, uniformly

	Shape	Activations	Epochs
Encoders	3 : 32 : 32 : 16 : 4 : 1	elu : elu : elu : elu : linear	1000
Decoders	1 : 4 : 16 : 32 : 32 : 3	elu : elu : elu : elu : linear	1000
Dynamics	1 : 32 : 32 : 16 : 4 : 1	elu : elu : elu : elu : linear	1000

TABLE II. Neural network parameters for periodic dynamics on a torus. “Shape” indicates the dimension of each layer, “activation” indicates the activation functions between layers, and “epochs” indicates the number of epochs used for training.

	Shape	Activations	Epochs
Encoders	3 : 32 : 64 : 32 : 16 : 4 : 2	elu : elu : elu : elu : elu : linear	2000
Decoders	2 : 4 : 16 : 32 : 64 : 32 : 3	elu : elu : elu : elu : elu : linear	2000
Dynamics	2 : 32 : 32 : 16 : 4 : 2	elu : elu : elu : elu : linear	2000

TABLE III. Neural network parameters for quasiperiodic dynamics on a torus. “Shape” indicates the dimension of each layer, “activation” indicates the activation functions between layers, and “epochs” indicates the number of epochs used for training.

spaced $3\pi/100$ radians apart in the toroidal direction, covering 15 full periods in the toroidal direction.

We use six charts (six clusters in k -means). The graph is built by connecting points to their five nearest neighbours. Clusters are expanded twice along the graph.

The neural network parameters are listed in table III. The autoencoders are trained with an exponential decay learning rate schedule (initial learning rate 0.01, decay rate 0.8 every 200 steps using a staircase function), and the neural networks for dynamics are also trained with an exponential decay learning rate schedule (initial learning rate 0.01, decay rate 0.9 every 200 steps using a staircase function).

S4. BEATING DYNAMICS

We compute a numerical solution to the Kuramoto-Sivashinsky equation,

$$u_t + uu_x + u_{xx} + \nu u_{xxxx} = 0, \tag{S2}$$

	Shape	Activations	Epochs
Encoders	64 : 128 : 64 : 16 : 8 : 1	elu : elu : elu : elu : linear	2000
Decoders	1 : 8 : 16 : 64 : 128 : 64	elu : elu : elu : elu : linear	2000
Dynamics	1 : 32 : 32 : 16 : 4 : 1	elu : elu : elu : elu : linear	2000

TABLE IV. Neural network parameters for beating dynamics of the Kuramoto-Sivashinsky equation. “Shape” indicates the dimension of each layer, “activation” indicates the activation functions between layers, and “epochs” indicates the number of epochs used for training.

for $0 \leq x \leq 2\pi$ with periodic boundary conditions using a pseudo-spectral method with 64 Fourier modes. Time integration is performed using Crank-Nicolson for the linear terms and two-step Adams-Bashforth for the nonlinear term. The first step of the time integration is performed using the fourth-order Runge-Kutta method. The time step used is 10^{-4} . The initial condition is $u(x, 0) = -\sin x + 2 \cos 2x + 3 \cos 3x - 4 \sin 4x$ [39].

We set $\nu = \frac{16}{337}$; once transients decay, we obtain a beating standing wave and collect our data. The training data are the values of the field u at 64 points spaced equally in x ; our dataset consists of 100 such data points, uniformly spaced 0.01 time units apart, covering a bit more than two periods of the beating wave.

We use three charts (three clusters in k -means). The graph is built by connecting points to their four nearest neighbours. Clusters are expanded once along the graph.

The neural network parameters are listed in table IV. The autoencoders are trained with an exponential decay learning rate schedule (initial learning rate 0.01, decay rate 0.8 every 200 steps using a staircase function), and the neural networks for dynamics are also trained with an exponential decay learning rate schedule (initial learning rate 0.01, decay rate 0.9 every 200 steps using a staircase function).

S5. BEATING TRAVELLING DYNAMICS

We compute a numerical solution to the Kuramoto-Sivashinsky equation as before. We set $\nu = \frac{4}{87}$; once transients decay, we obtain a beating travelling wave and collect our data. The training data are the values of the field u at 64 points spaced equally in x ; our dataset consists of 100 such data points, uniformly spaced 0.01 time units apart, covering a bit more than two beating periods and 1% of the travelling period. Separation of the data into shape

	Shape	Activations	Epochs
Encoders	64 : 128 : 64 : 16 : 8 : 1	elu : elu : elu : elu : linear	2000
Decoders	1 : 8 : 16 : 64 : 128 : 64	elu : elu : elu : elu : linear	2000
Shape dynamics	1 : 32 : 32 : 16 : 4 : 1	elu : elu : elu : elu : linear	2000
Phase dynamics	1 : 32 : 32 : 16 : 4 : 1	elu : elu : elu : elu : linear	2000

TABLE V. Neural network parameters for beating travelling dynamics of the Kuramoto-Sivashinsky equation. “Shape” indicates the dimension of each layer, “activation” indicates the activation functions between layers, and “epochs” indicates the number of epochs used for training.

and phase variables is described in the main text.

We use three charts (three clusters in k -means). The graph is built by connecting points to their four nearest neighbours. Clusters are expanded twice along the graph.

The neural network parameters are listed in table V. The autoencoders are trained with an exponential decay learning rate schedule (initial learning rate 0.01, decay rate 0.9 every 200 steps using a staircase function), the neural networks for shape dynamics are also trained with an exponential decay learning rate schedule (initial learning rate 0.01, decay rate 0.9 every 200 steps using a staircase function), and the neural networks for phase dynamics are also trained with an exponential decay learning rate schedule (initial learning rate 0.01, decay rate 0.9 every 200 steps using a staircase function).

S6. BURSTING DYNAMICS

We compute a numerical solution to the Kuramoto-Sivashinsky equation as before. We set $\nu = \frac{16}{71}$; once transients decay, we obtain bursting dynamics and collect our data. The training data are the values of the field u at 64 points spaced equally in x ; our dataset consists of 6565 such data points, uniformly spaced 0.05 time units apart, covering 16 bursts.

The data described above are used to train the autoencoders. The neural networks for dynamics are trained using a different dataset. To create the dynamics dataset, we took every third data point of the autoencoder dataset (2189 in total), perturbed them, and used the resulting data as initial conditions for new simulations. The perturbations are given by

$$a_1 \cos 2x + a_2 \cos x + a_3 \sin x, \tag{S3}$$

	Shape	Activations	Epochs
Encoders	64 : 128 : 64 : 16 : 8 : 3	elu : elu : elu : elu : linear	1000
Decoders	3 : 8 : 16 : 64 : 128 : 64	elu : elu : elu : elu : linear	1000
Shape dynamics	3 : 16 : 64 : 64 : 16 : 3	elu : elu : elu : elu : linear	1000

TABLE VI. Neural network parameters for bursting dynamics of the Kuramoto-Sivashinsky equation. “Shape” indicates the dimension of each layer, “activation” indicates the activation functions between layers, and “epochs” indicates the number of epochs used for training.

where the a_i are randomly sampled from a uniform distribution spanning $[-0.05, 0.05]$. The new simulations were all run for 1.5 time units, and only the last time unit of data was stored. In the end, our dynamics dataset consists of 2189 slightly-off-attractor trajectories, each spanning one time unit and consisting of 21 data points uniformly spaced 0.05 time units apart.

We use six charts (six clusters in k -means). The graph is built by connecting points to their four nearest neighbours. Clusters are expanded twice along the graph.

The neural network parameters are listed in table VI. For the autoencoders, we use the method described in [6] with $\alpha = 1$ (cf. eq. 4 in that work). The autoencoders are trained with an exponential decay learning rate schedule (initial learning rate 0.01, decay rate 0.8 every 200 steps using a staircase function), and the neural networks for dynamics are also trained with an exponential decay learning rate schedule (initial learning rate 0.01, decay rate 0.9 every 200 steps using a staircase function).

In this example, we add an additional step before learning the dynamics, which we referred to as normalization in the main text. In each chart, we take the training data in their local coordinates, subtract the mean, and perform principal components analysis (PCA), changing the local coordinates to their coordinates in the PCA basis (without any dimension reduction). We then normalize each PCA coordinate by the data’s standard deviation along the coordinate. This set of steps is similar to whitening. We found this type of normalization to be helpful in learning accurate dynamics. The rationale for normalizing the local coordinates before learning the dynamics is that the saddle points have sharp cusps leading into them, and we thought normalizing the local coordinates would make the cusps less sharp and therefore make the sensitive dynamics easier to learn.